Advances in Mathematical
Sciences and Applications
Vol. 28, No. 2 (2019), pp. 413–424

GAKKOTOSHO
TOKYO JAPAN

NUMERICAL REALIZATION OF A NEW GENERATION TOMOGRAPHY ALGORITHM BASED ON THE CAUCHY-TYPE INTEGRAL FORMULA

Hiroshi Fujiwara
Graduate School of Informatics, Kyoto University
Yoshida-honmachi, Sakyo-ku, Kyoto, 606-8501, Japan
(E-mail: fujiwara@acs.i.kyoto-u.ac.jp)

and

Alexandru Tamasan
Department of Mathematics, University of Central Florida
Orlando, Florida, 32816, USA
(E-mail: tamasan@math.ucf.edu)

Abstract. This work concerns the numerical realization of a Cauchy-type integral formula for sequence valued analytic functions in the sense of Bukhgeim, and its applications to the source reconstruction problem in inverse radiative transport through a non-absorbing and non-scattering medium. The inverse source problem is mathematically equivalent to the classical X-ray Computed Tomography (CT), where a function is to be determined from its line integrals. The proposed algorithms have the added advantage to extend to the source determination problems in media with absorbing and scattering properties. Such extensions cannot be achieved in the existing X-ray CT algorithms. The numerical experiments demonstrate the feasibility of our new tomographic algorithms.

Communicated by Hitoshi Imai; Received August 6, 2019.
The first author was supported by JSPS KAKENHI Grant Numbers 16H02155, 18K18719, and 18K03436.
The second author was supported in part by the NSF grant DMS-1907097.
AMS Subject Classification: 65N21, 30E20, 92C55.
Keywords: transport equation, inverse problems, numerical source reconstruction.

1 Introduction

In this work we propose new numerical algorithms for the quantitative source determination in an inverse boundary value problem for stationary radiative transfer, which is applicable and extensible to a broad range of non-destructive imaging methods.

The boundary value problem of the stationary transport equation

$$\xi \cdot \nabla_x I(x,\xi) = q(x), \qquad x \in \Omega,\ \xi \in S^1, \tag{1a}$$

$$I(x,\xi) = 0, \qquad (x,\xi) \in \Gamma_-, \tag{1b}$$

models a beam of particles generated by the source q and propagating without attenuation and scattering in a domain $\Omega \subset \mathbb{R}^2$. The planar domain Ω is bounded and strictly convex with smooth boundary, while $S^1 = \{\xi \in \mathbb{R}^2\,;\, |\xi| = 1\}$ is the unit circle of directions. We pose outflow and inflow boundaries as $\Gamma_\pm = \{(x,\xi)\,;\, x \in \partial\Omega, \xi \in S^1, \nu(x)\cdot\xi \gtrless 0\}$ where $\nu(x)$ is the outer unit normal to $\partial\Omega$. The quantity $I(x,\xi)$ represents the particle density at the position $x \in \Omega$ with velocity $\xi \in S^1$. Equation (1b) means that no radiation is entering the domain from the exterior. The particle source term is assumed square integrable, $q \in L^2(\Omega)$, and compactly supported in Ω.

We consider here the following inverse source problem: Find q in Ω from measurements of the outflow at the boundary:

$$I(x,\xi) = I_{\text{measure}}(x,\xi), \qquad (x,\xi) \in \Gamma_+. \tag{2}$$

Due to the convexity of the domain, for each $(x,\xi) \in (\Omega \times S^1) \cup \Gamma_+$, there exists a unique intersection point $x_- = x_-(x,\xi)$ of the boundary with the semi axis starting from x in the opposite direction of ξ. In particular, if $s = s(x,\xi)$ denote the distance from x to x_-, then $x = x_- + s\xi$. For each $\xi \in S^1$, (1a) is an ODE along the line through x_- in the ξ-direction, whose solution is given by the integral

$$I(x,\xi) = I(x_- + s\xi, \xi) = \int_0^s q(x_- + t\xi)\, dt. \tag{3}$$

If $(x,\xi) \in \Gamma_+$, then $I(x,\xi) = \displaystyle\int_{-\infty}^{\infty} q(x + t\xi)\, dt$ ($q \equiv 0$ outside domain), and the inverse source problem is equivalent to the inversion of the Radon transform problem [11]. The latter is the mathematical model of X-ray Computed Tomography (CT). In the typical CT setting, the measured data (*sinogram*) is equivalent to our boundary information I_{measure}.

While the conventional X-ray CT algorithms [8, 9, 10] do provide the solution to the inverse source problem considered here, they do not extend to the case where the particle beam is attenuated and scattered by medium. As a result, applications of the X-ray CT imaging techniques to Positron Emission Tomography (PET) produce low-resolution images, because the latter involves both attenuation and scattering.

This paper proposes new algorithms for the source reconstruction problem for the transport equation and demonstrates their numerical feasibility. The proposed algorithms are based on a Cauchy-type boundary integral formula corresponding to analytic sequence valued maps as originally introduced by A. Bukhgeim [1]. We mention here that the

proposed method can be extended to transport through an absorbing and scattering media. Such extensions are investigated in a forthcoming publication [7].

In the next section, we briefly sketch the mathematical reconstruction procedure based on the Bukhgeim-Cauchy integral formula in (5) below. In Section 3 we propose two numerical algorithms for source reconstructions. Finally, in Section 4, several numerical experiments are conducted to demonstrate the effectiveness of our algorithms.

2 Mathematical Formulation

We summarize the mathematical reconstruction procedure to the non-attenuation problem (1) from [1, 7], which should be referred to for rigorous setting and proofs. Throughout the paper, $x = (x_1, x_2) \in \mathbb{R}^2$ is identified with $z = x_1 + ix_2 \in \mathbb{C}$ with $i = \sqrt{-1}$. Also, $\xi = \xi(\theta) = (\cos\theta, \sin\theta) \in S^1$ is identified with $0 \le \theta < 2\pi$. We also denote an interior point of Ω by z, whereas ζ indicates a boundary point.

For any $q \in L^2(\Omega)$, the forward boundary value problem problem (1) has unique solution I given by (3). Moreover, the solution

$$I \in W^2(\Omega \times S^1) := \{f \in L^2(\Omega \times S^1)\,;\, (x,\xi) \mapsto \xi \cdot \nabla_x f(x,\xi) \in L^2(\Omega \times S^1)\},$$

and its trace $I|_{\Gamma_+} \in L^2(\Gamma_+)$, see [3].

By the operators $\partial = (\partial_{x_1} - i\partial_{x_2})/2$ and $\overline{\partial} = (\partial_{x_1} + i\partial_{x_2})/2$, we have $\xi \cdot \nabla_x = e^{-i\theta}\overline{\partial} + e^{i\theta}\partial$, and thus the transport equation (1a) becomes

$$e^{-i\theta}\overline{\partial} I + e^{i\theta}\partial I = q.$$

Since the Fourier series $I(z,\xi) = \sum_{n\in\mathbb{Z}} I_n(z) e^{-in\theta}$ converges (in the L^2 sense) a.e. $z \in \Omega$, we have

$$\sum_{n\in\mathbb{Z}} \overline{\partial} I_n(z) e^{-i(n+1)\theta} + \sum_{n\in\mathbb{Z}} \partial I_n(z) e^{-i(n-1)\theta} = q(z).$$

From homogeneity of q and the orthogonality of $\{e^{in\theta}\}$ the equation above reduces to the system

$$\overline{\partial} I_{-1} + \partial I_1 = q, \quad \text{and} \quad \overline{\partial} I_n + \partial I_{n+2} = 0, \qquad n \neq -1.$$

As I is a real valued function, we have $\overline{I_n} = I_{-n}$ for $n \in \mathbb{Z}$. Therefore it is sufficient to consider

$$\overline{\partial} I_{-1} + \partial I_1 = q, \tag{4a}$$

$$\overline{\partial} I_n + \partial I_{n+2} = 0, \qquad n = 0, 1, 2, \ldots . \tag{4b}$$

The values $\{I_n\}$ which solves the system (4b) are determined from the boundary values. More precisely, for $n \ge 0$, $I_n(z)$ is given by the Bukhgeim-Cauchy formula [1, 4]:

$$\begin{aligned} I_n(z) = {} & \frac{1}{2\pi i} \int_{\partial\Omega} \frac{I_n(\zeta)}{\zeta - z}\, d\zeta \\ & + \frac{1}{2\pi i} \int_{\partial\Omega} \left\{ \frac{d\zeta}{\zeta - z} - \frac{d\overline{\zeta}}{\overline{\zeta} - \overline{z}} \right\} \sum_{j=1}^{\infty} I_{n+2j}(\zeta) \left(\frac{\overline{\zeta} - \overline{z}}{\zeta - z} \right)^j, \qquad z \in \Omega. \end{aligned} \tag{5}$$

Note that the right hand side depends only on the boundary values of I_n, and they are determined from the measurement on the outflow boundary (2) and the zero inflow condition (1b). Therefore $I_1(z)$, $z \in \Omega$, is obtained. Moreover, if $\partial\Omega$ has a parameterization $\zeta(\omega)$, $0 \le \omega < 2\pi$, then the integral in the second term on the right hand side is simplified for the purpose of numerical computation as

$$\frac{1}{2\pi i}\int_{\partial\Omega}\left(\frac{d\zeta}{\zeta - z} - \frac{d\overline{\zeta}}{\overline{\zeta} - \overline{z}}\right) F(\zeta) = \frac{1}{\pi}\int_0^{2\pi} \operatorname{Im}\left(\frac{\zeta'(\omega)}{\zeta(\omega) - z}\right) F\big(\zeta(\omega)\big)\, d\omega.$$

with F being the series in (5). Finally from $I_{-1} = \overline{I_1}$ and (4a), the unknown source $q(z)$, $z \in \Omega$, is reconstructed.

3 Numerical Algorithms

This section gives two numerical reconstruction procedures based on the last section. Both algorithms reconstruct the source term q as a piecewise-constant function with respect to triangles forming a triangulation of Ω.

Algorithm P0. Assume that $\partial\Omega$ has a parameterization $\zeta(\omega)$, $0 \le \omega < 2\pi$, and that I_{measure} is given on Γ_+. Three positive integers, N, K, and M are used in discretization. We also introduce an inscribed polygonal domain $\Omega_h \approx \Omega$, and generate a triangulation $\mathcal{T} = \{\tau_\ell\}$ of Ω_h, i.e. each τ_ℓ is a triangle, $\tau_\ell \cap \tau_k = \emptyset$ if $\ell \ne k$, and $\overline{\Omega_h} = \bigcup_\ell \overline{\tau_\ell}$.

Step P0-1. Let $\theta_n = 2\pi n/N$ for $0 \le n < N$, and $\omega_k = 2\pi k/K$ for $0 \le k \le K$. Write $\zeta_k = \zeta(\omega_k)$ and $\zeta_k' = \zeta'(\omega_k)$ for $0 \le k < K$. Compute

$$\mathcal{I}_{1+2m,k} = \frac{1}{N}\sum_{n=0}^{N-1} \tilde{I}_{\text{measure}}\big(\zeta_k, \xi(\theta_n)\big) e^{i(1+2m)\theta_n},$$

for $1 \le 1 + 2m \le M$ and $0 \le k < K$, where

$$\tilde{I}_{\text{measure}}(\zeta, \xi) = \begin{cases} I_{\text{measure}}(\zeta, \xi), & \text{if } (\zeta, \xi) \in \Gamma_+; \\ 0, & \text{otherwise.} \end{cases}$$

This obviously arises from the composite trapezoidal rule to the Fourier transform

$$I_{1+2m}(\zeta_k) = \frac{1}{2\pi}\int_0^{2\pi} I\big(\zeta_k, \xi(\theta)\big) e^{i(1+2m)\theta}\, d\theta.$$

In other words, I_{measure} is sampled at $\big(\zeta_k, \xi(\theta_n)\big) \in \Gamma_+$. Since the source is compactly supported inside, we also use $I(\zeta, \xi) = 0$ for $\nu(\zeta) \cdot \xi = 0$.

Step P0-2. Let z_ℓ be the center of mass of τ_ℓ and write C as the set of centers. For $z_\ell \in C$, compute $\mathcal{I}_1(z_\ell)$, where

$$\mathcal{I}_1(z) = \frac{1}{Ki}\sum_{k=0}^{K-1}\frac{\zeta_k'}{\zeta_k - z}\mathcal{I}_{1,k} + \frac{2}{K}\sum_{k=0}^{K-1}\left\{\mathrm{Im}\left(\frac{\zeta_k'}{\zeta_k - z}\right)\right\}\left\{\sum_{m=1}^{\lfloor (M-1)/2\rfloor}\mathcal{I}_{1+2m,k}\left(\frac{\overline{\zeta_k} - \overline{z}}{\zeta_k - z}\right)^m\right\}, \qquad z \in \Omega. \quad (6)$$

This approximates (5). Note that the denominator $\zeta_k - z$ never vanishes because $z \in \Omega$ and $\zeta_k \in \partial\Omega$.

Step P0-3. For each τ_ℓ, we evaluate partial derivatives $\partial_{x_1} I_1|_{\tau_\ell}$ and $\partial_{x_2} I_1|_{\tau_\ell}$. Suppose that τ_ℓ has three adjacent triangles τ_{ℓ_j}, of respective center of mass z_{ℓ_j}, and let denote by $(\lambda_{\ell_j,1}, \lambda_{\ell_j,2}) = \big(\mathrm{Re}(z_{\ell_j} - z_\ell), \mathrm{Im}(z_{\ell_j} - z_\ell)\big)$ the corresponding displacements, $j = 1, 2, 3$. Solve

$$\begin{pmatrix} \lambda_{\ell_1,1} & \lambda_{\ell_1,2} \\ \lambda_{\ell_2,1} & \lambda_{\ell_2,2} \\ \lambda_{\ell_3,1} & \lambda_{\ell_3,2} \end{pmatrix} \begin{pmatrix} \delta_{x_1}\mathcal{I}_1(z_\ell) \\ \delta_{x_2}\mathcal{I}_1(z_\ell) \end{pmatrix} = \begin{pmatrix} \mathcal{I}_1(z_{\ell_1}) - \mathcal{I}_1(z_\ell) \\ \mathcal{I}_1(z_{\ell_2}) - \mathcal{I}_1(z_\ell) \\ \mathcal{I}_1(z_{\ell_3}) - \mathcal{I}_1(z_\ell) \end{pmatrix} \quad (7)$$

in the sense of least square. For each z_ℓ, there exists a unique solution, $\delta_{x_1}\mathcal{I}_1(z_\ell)$ and $\delta_{x_2}\mathcal{I}_1(z_\ell)$, since at least two of $z_{\ell_j} - z_\ell$, $j = 1, 2, 3$, are linearly independent. If τ_ℓ has two adjacent triangles, they can be calculated similarly.

Step P0-4. For each triangle $\tau_\ell \in \mathcal{T}$, (4a) gives the reconstruction of $q|_{\tau_\ell}$ as

$$q_\ell = \mathrm{Re}\big(\delta_{x_1}\mathcal{I}_1(z_\ell)\big) + \mathrm{Im}\big(\delta_{x_2}\mathcal{I}_1(z_\ell)\big).$$

Remark. We give a remark on Step P0-3. The directional derivative of a smooth function $f(z)$ to the direction $\nu = (\nu_1, \nu_2)$ (a unit vector) is given by

$$\frac{\partial f}{\partial \nu}(z_\ell) = \frac{\partial f}{\partial x_1}(z_\ell)\nu_1 + \frac{\partial f}{\partial x_2}(z_\ell)\nu_2.$$

We approximate this observation; discretizing the directional derivative on the left hand side by the finite difference, we obtain the system

$$\frac{\mathcal{I}_1(z_{\ell_j}) - \mathcal{I}_1(z_\ell)}{\|\lambda_{\ell_j}\|} = \delta_{x_1}\mathcal{I}_1(z_\ell)\frac{\lambda_{\ell_j,1}}{\|\lambda_{\ell_j}\|} + \delta_{x_2}\mathcal{I}_1(z_\ell)\frac{\lambda_{\ell_j,2}}{\|\lambda_{\ell_j}\|}, \qquad j = 1, 2, 3,$$

that is (7). This insight infers that $\delta_{x_1}\mathcal{I}_1(z_\ell)$ and $\delta_{x_2}\mathcal{I}_1(z_\ell)$ are expected to approximate the partial derivatives $\partial_{x_1} I_1(z_\ell)$ and $\partial_{x_2} I_1(z_\ell)$ respectively.

Same procedure is applicable to a rectangulation by a regular lattice instead of triangulations, where the solution coincides with the central difference.

In Algorithm P0, $I_1(z)$ is approximated by a piecewise constant function, which is reasonable if $I_1 \in L^2(\Omega)$. However, for smoother sources, algorithms based on smoother approximation are expected to increase the accuracy. Such examples motivate the next algorithm.

Algorithm P1. Suppose that the same discretization parameters as Algorithm P0 are given. A triangulation is also required.

Step P1-1. Same as Step P0-1.

Step P1-2. Let V be the set of the vertices of the triangulation $\mathcal{T}$. For $v_j \in V \cap \Omega$, compute an approximation to $I(v_j)$ by $\mathcal{I}_1(v_j)$ in (6). For $v_j \in V \cap \partial\Omega$, we let $\mathcal{I}_1(v_j) = \mathcal{I}_{1,k}$ where $v_j = \zeta_k \in \partial\Omega$. Note that I_{measure} is also sampled at $V \cap \partial\Omega$.

Step P1-3. Denote vertices of a triangle τ_ℓ by v_{ℓ_j}, $j = 1, 2, 3$. Find a linear function $\varphi_{\tau_\ell}(x_1, x_2) = a_\ell x_1 + b_\ell x_2 + c_\ell$, $a_\ell, b_\ell, c_\ell \in \mathbb{C}$, subject to $\varphi_{\tau_\ell}(v_{\ell_j}) = \mathcal{I}_1(v_{\ell_j})$ for $j = 1, 2, 3$. This means that $I_1(z)$ is approximated by a continuous and piecewise-linear function. Note that φ_{τ_ℓ} uniquely exists on each τ_ℓ.

Step P1-4. Finally the source in τ_ℓ is reconstructed as

$$q_\ell = \mathrm{Re}(a_\ell) + \mathrm{Im}(b_\ell).$$

4 Numerical Experiments

In this section, we exhibit numerical examples by the proposed algorithms. In the examples, the target source $q(x)$ is assigned by the modified Shepp-Logan model [12], which occupies the ellipse

$$\Omega = \left\{ (x_1, x_2)\,;\, \frac{x_1^2}{a^2} + \frac{x_2^2}{b^2} < 1 \right\}, \quad a = 0.69, b = 0.92,$$

and thus $\partial\Omega = \{(a\cos\omega, b\sin\omega); 0 \le \omega < 2\pi\}$. Throughout this section, the discretization parameters are $K = 360$, $N = 360$, and $M = 128$. The triangulation $\mathcal{T}$ is generated without any information of inclusions, and it consists of 12132 vertices and 23862 triangles The maximum diameter of the triangulation is 0.0237. We write by z_l the center of mass of each triangle $\tau_\ell \in \mathcal{T}$. All computations are processed with the double precision arithmetic.

Firstly, the boundary data $I|_{\Gamma_- \cup \Gamma_+}$ is represented in Figure 1. For each $\zeta \in \partial\Omega$ (indicated by $\bullet$), the graph $\left\{ \big(I(\zeta, \xi), \xi\big)\,;\, \xi \in S^1 \right\}$ is shown as the closed curve in the polar coordinates $\left\{ \zeta + \frac{1}{2} I(\zeta, \xi)\xi\,;\, \xi \in S^1 \right\}$ [5]. Note that, since $I|_{\Gamma_-} = 0$ (no incoming radiation (1b)), the curve never enters the domain Ω indicated by the gray area. The boundary observation I_{measure} is equivalent to the Radon transform shown by sinogram (Figure 2) as mentioned earlier, which gives complete measurement data. On the contrary, Figure 1 gives more instinctive understanding.

Reconstructed q by Algorithm P0 and Algorithm P1 are depicted in Figure 3 and Figure 4 respectively. Each equips the section on the dotted segment, and they shows that the reconstructed results shows quantitative agreements.

In order to estimate directional derivatives in Step P0-3, we also compute q by the finite difference, replacing Step P0-3 and P0-4,

$$q_\ell = \mathrm{Re}\,\frac{\mathcal{I}_1(z_\ell + h) - \mathcal{I}_1(z_\ell - h)}{2h} + \mathrm{Im}\,\frac{\mathcal{I}_1\big(z_\ell + h\sqrt{-1}\big) - \mathcal{I}_1\big(z_\ell - h\sqrt{-1}\big)}{2h},$$

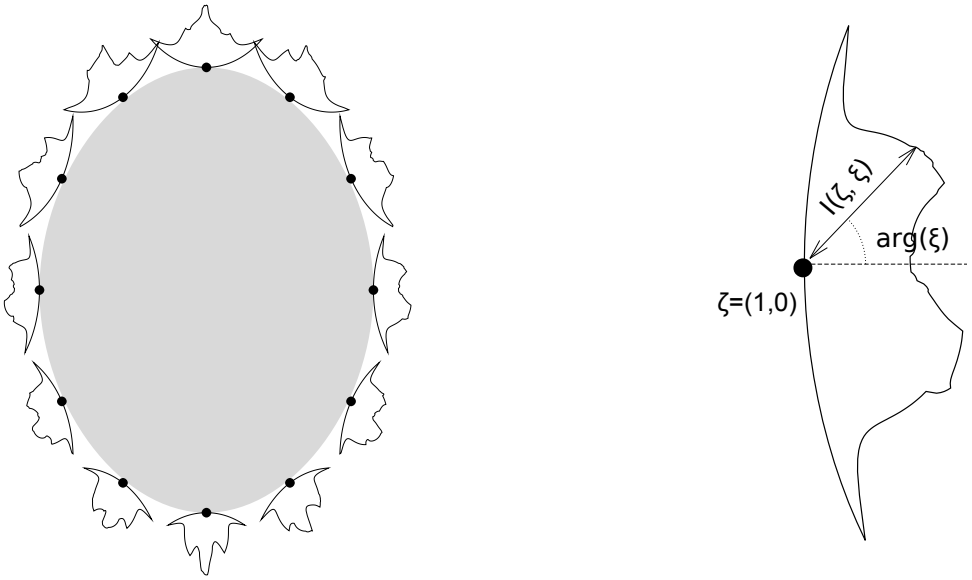

Figure 1: Boundary data $I(\zeta,\xi)|_{\Gamma_-\cup\Gamma_+}$. The curve is $\left\{\zeta+\frac{1}{2}I(\zeta,\xi)\xi\,;\,\xi\in S^1\right\}$ for $\zeta\in\partial\Omega$ indicated by the dot ($\bullet$). The Shepp-Logan model occupies the gray area. The right figure is a magnification of that at $\zeta=(1,0)$.

Table 1: Computational times, unit: sec.

Algorithm	Total	Fourier coefficient (Step P0-1 and P1-1)	Numerical integration (6) and others (ratio)
Algorithm P0	5.43	1.60	3.83 (1.95)
Algorithm P1	3.50	1.61	1.96 (1)
Algorithm FD	16.8	1.62	15.2 (7.76)

where $h\approx 0.00806$ is the average of distances between centers of mass of adjacent triangles (we call this Algorithm FD [6]). The numerical result is depicted in Figure 5. Table 1 shows computational times on Xeon E5-2650 v4 (2.2GHz) with single core. Theoretically computational times of Algorithm P0 and Algorithm FD are proportional to number of triangles, while those of Algorithm P1 is proportional to that of vertices. In numerical experiments, the ratios shown inside parenthesis $(\cdot)$ in Table 1 agree with ideal ratios.

We evaluate a pseudo-error of a reconstructed $\{q_\ell\}$ by

$$E_q(\mathcal{T})=\left\{\sum_{\tau_\ell\in\mathcal{T}}|q(z_\ell)-q_\ell|^2\,|\tau_\ell|\right\}^{1/2},$$

where $|\tau_\ell|$ is the area of τ_ℓ. Note that $E_q(\mathcal{T})$ does not give L^2-error because all inclusions in the Shepp-Logan model are not polygons but ellipses, and thus the exact $q(z)$ can be discontinuous on some triangles. The evaluated values for Algorithm P0, Algorithm P1,

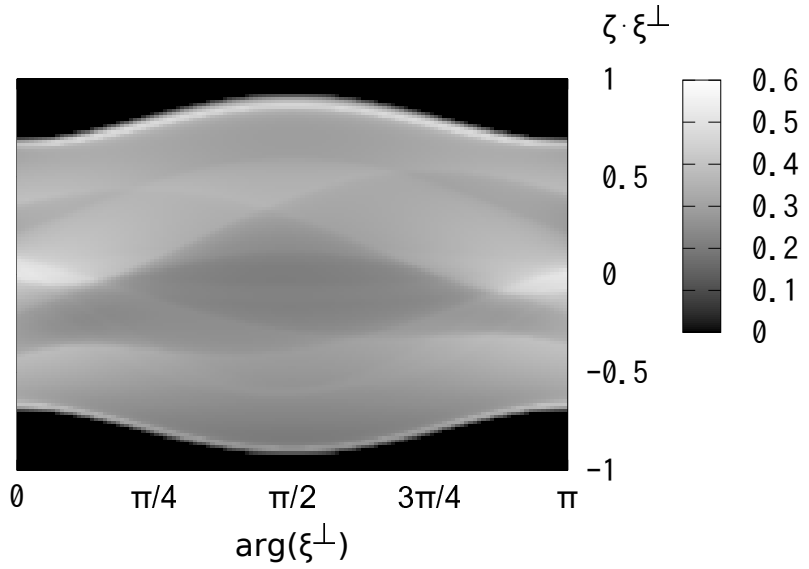

Figure 2: Sinogram representing measurement data (the Radon transform) for the modified Shepp-Logan model [12]

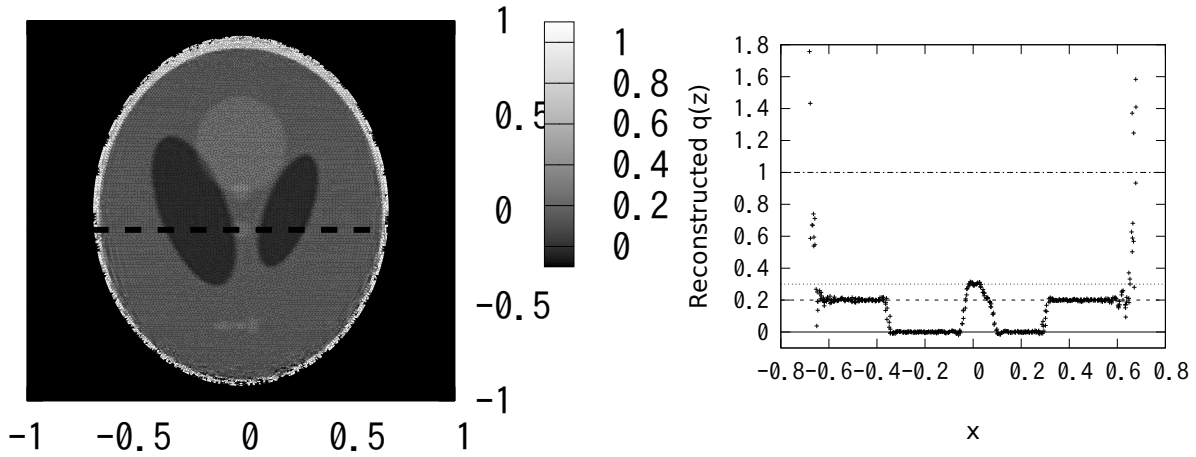

Figure 3: Reconstructed q_ℓ by Algorithm P0 on Ω (left) and its section on the dotted line (right)

and Algorithm FD are 0.939, 0.162, and 6.44 respectively. Relatively larger disturbance are observed in the profile of Algorithm FD.

Figure 6 plot the reconstructed q_ℓ with z_ℓ in $0.98^2 \leq (x_1/a)^2 + (x_2/b)^2 \leq 0.99^2$ by the algorithms. The averages of Algorithm P0, Algorithm P1 and Algorithm FD are 1.09, 0.97, and 1.47, respectively. The exact value in this annual domain is 1, thus the proposed algorithms are observably accurate than the finite difference.

In order to analyze disturbance more precisely, errors in Bukhgeim-Cauchy integral

$$\mathrm{Error}(r) = \max_{z \in \partial\Omega(r)} \left| \frac{1}{J} \sum_{j=0}^{J-1} I\big(z, \xi(\theta_j)\big) e^{i\theta_j} - \mathcal{I}_1(z) \right|, \tag{8}$$

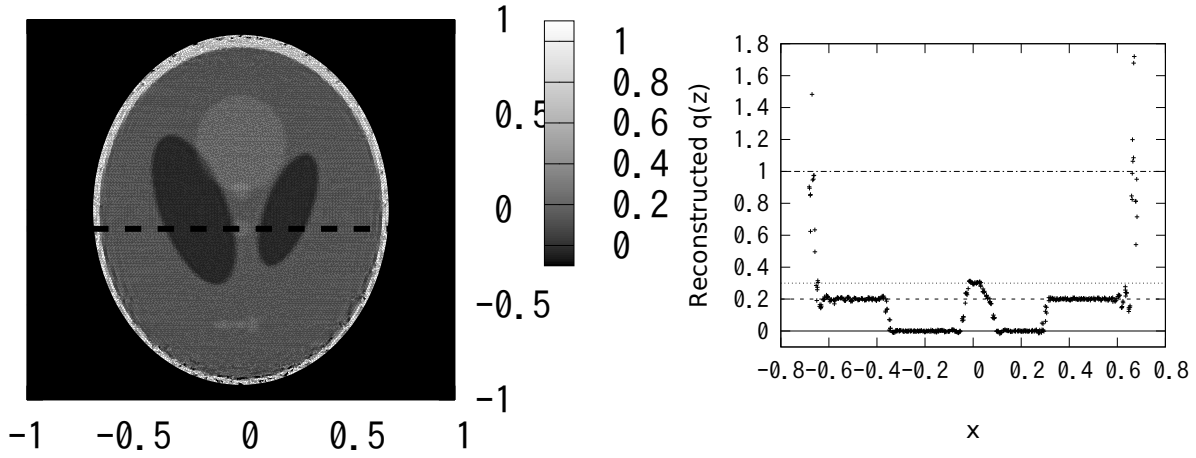

Figure 4: Reconstructed q_ℓ by Algorithm P1 on Ω (left) and its section on the dotted line (right)

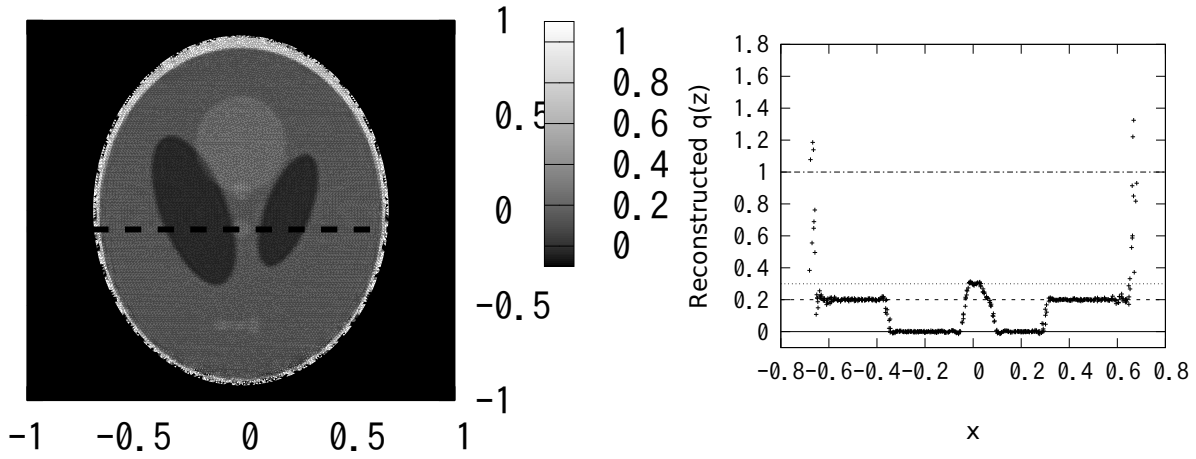

Figure 5: Reconstructed q_ℓ by Algorithm FD [6] on Ω (left) and its section on the dotted line (right)

where $\partial\Omega(r) = \{z \in \Omega\,;\, \mathrm{dist}(z, \partial\Omega) = r\}$ and where $J = 2048$, is shown in Figure 7. For each distance r, we compute 360000 equi-spaced points for the argument direction; we check the maximum among $z = \rho_n \exp(i\eta_n) \in \partial\Omega(r)$ with $\eta_n = 2\pi n/360000$, $n \in \mathbb{Z}$. From the results, errors in computation of (5) grow in $O(1/r)$ as z approaches to $\partial\Omega$. This inaccuracy near the boundary occurs from the near singular kernel $1/(\zeta - z)$, $\zeta \in \partial\Omega$, $z \in \Omega$, and it is accumulated by cancellation in differentiations. Note that if we change J to 4096, the results are almost same. This means that the discrete Fourier transform $\dfrac{1}{J}\displaystyle\sum_{j=0}^{J-1} I\big(z, \xi(\theta_j)\big)e^{i\theta_j}$ is calculated sufficiently accurate.

Finally Figure 8 depicts behaviors of $E_q(\mathcal{T})$ for the algorithms with $K = 360$, $N = 360$ and $N = 128$ for several finer and coarser triangulations. From the figures, Algorithm P1 gives relatively accurate results. It also indicates that finer triangulations do not have

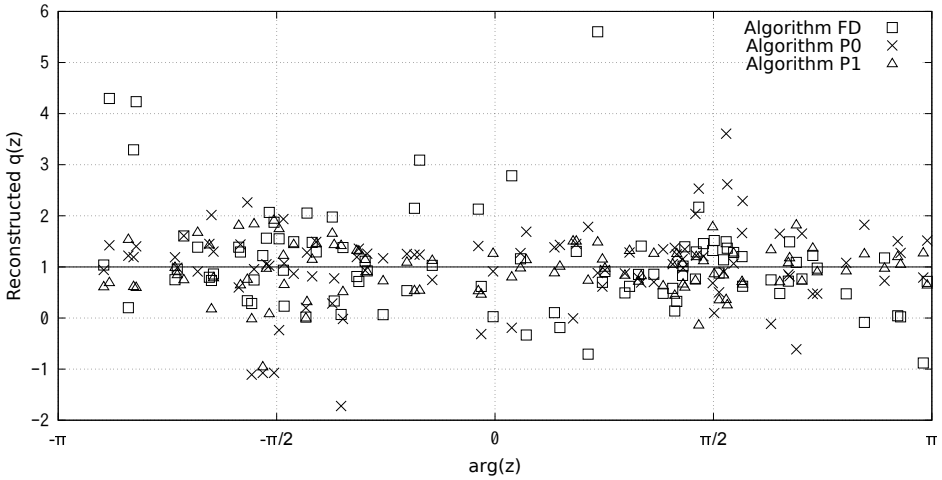

Figure 6: Reconstructed q_ℓ near $\partial\Omega$, $0.98^2 \leq (x_1/a)^2 + (x_2/b)^2 \leq 0.99^2$ with three differentiation algorithms. The averages of Algorithm P0 ($\times$) : 1.09, Algorithm P1 ($\triangle$): 0.97, Algorithm FD ($\square$) : 1.47. The exact value is 1.

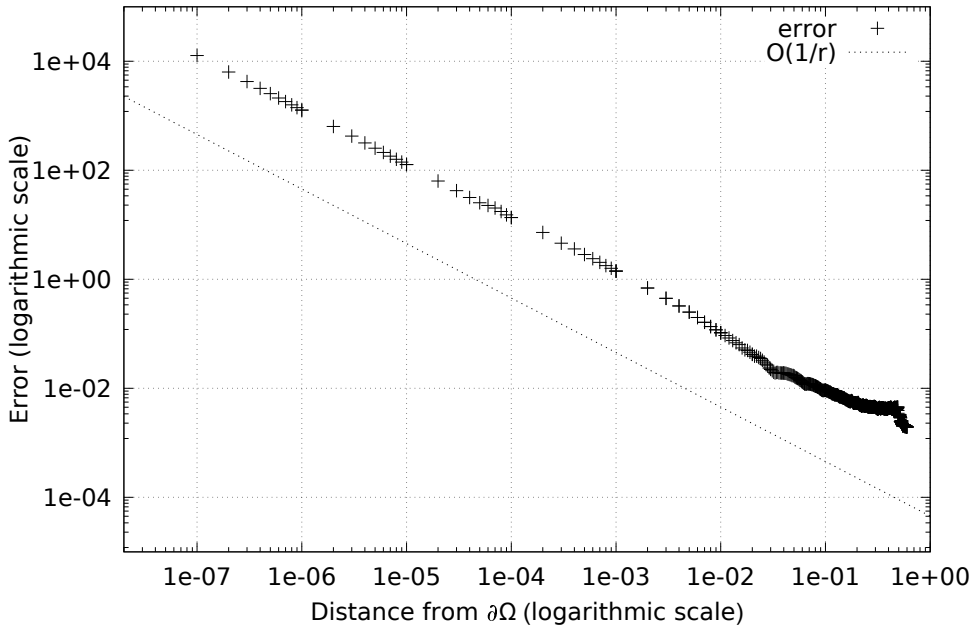

Figure 7: Errors (8) in Cauchy-type integral formula (6)

sense with fixed parameters K, N, and M. The results also indicate that the accuracy of the proposed Algorithm P0 and Algorithm P1 is not affected so much by triangulations, although Algorithm FD is.

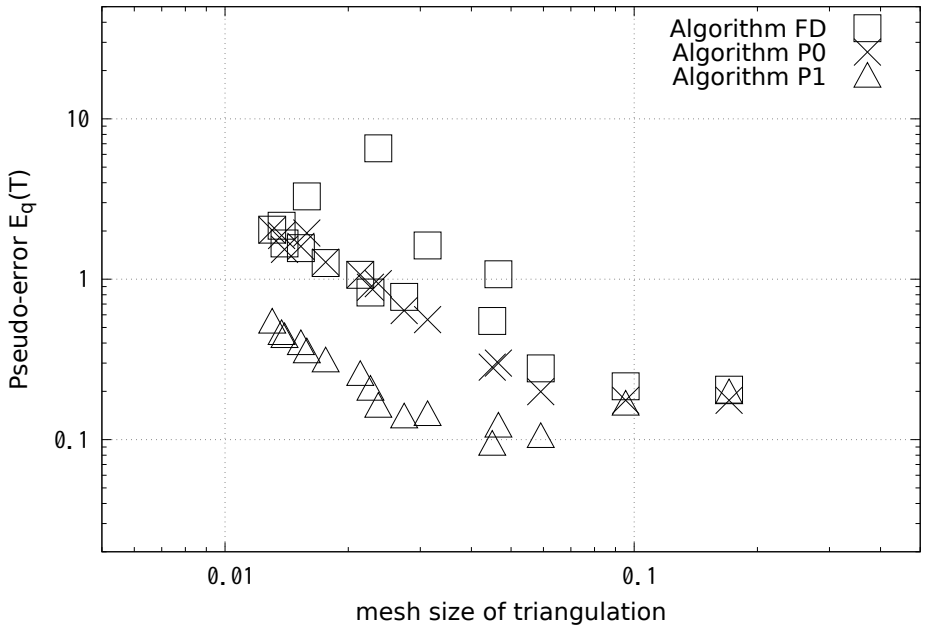

Figure 8: Behavior of pseudo-error $E_q(\mathcal{T})$ versus mesh size of triangulation $\mathcal{T}$

5 Concluding Remarks

Two numerical algorithms are proposed and investigated for the quantitative reconstruction of the source term in the boundary value problem of the transport equation. Numerical tests support the feasibility of the proposed methods in the case of reconstructing discontinuous sources. The proposed algorithms are fast and relatively more accurate than the finite difference algorithm.

The method relies on the computation of the Cauchy type integrals in (5), whose kernels become nearly singular for points close to the boundary. Several numerical methods to circumvent the inaccuracy at such points have been proposed, and shown to mitigate the reconstruction. However, the strength of the method is that the inaccuracy at the points nearby the boundary does not propagate to the computation at the interior points.

References

[1] A. L. Bukhgeim, *Inversion Formulas in Inverse Problems*, Linear Operators and Ill-Posed Problems by M. M. Lavrentiev and L. Ya. Savalev, Plenum, New York, 1995, pp. 323–378.

[2] A. L. Bukhgeim and A. A. Bukhgeim, *Inversion of the Radon Transform, Based on the The Theory of A-analytic Functions, with Application to 3D Inverse Kinematic Problem with Local Data*, J. Inverse Ill-Posed Probl., **14** (2006), pp. 219–234.

[3] M. Cessenat, *Théorèmes de trace L^p pour des espaces de fonctions de la neutronique*, C. R. Acad. Sci. Paris, Série I., **300** (1985), pp. 831–834.

[4] D. V. Finch, *The Attenuated X-ray Transform: Recent Developments*, in Inside Out: Inverse Problems and Applications, Math. Sci. Res. Inst. Publ., **47**, Cambridge Univ. Press, Cambridge, 2003, pp. 47–66.

[5] H. Fujiwara, *Fast Numerical Computation for the Stationary Radiative Transport Equation Using Multigrid Methods*, JASCOME, **11** (2011), pp. 13–18.

[6] H. Fujiwara and A. Tamasan, *Meshless X-ray Computerized Tomography by the Cauchy-type Integral Formula*, under review.

[7] H. Fujiwara, K. Sadiq, and A. Tamasan, *A Fourier Approach to the Inverse Source Problem in an Absorbing and Non-weakly Scattering Medium*, `arXiv:1907.07423` [math.AP], under review.

[8] S. Helgason, *The Radon Transform*, Progress in Mathematics **5**, Birkhäuser, Boston, 1980.

[9] D. Ludwig, *The Radon Transform on Euclidean Space*, Comm. Pure Appl. Math., **19** (1966), pp. 49–81.

[10] F. Natterer, *The Mathematics of Computerized Tomography*, Wiley, New York, 1986.

[11] J. Radon, *Über die Bestimmung von Funktionen durch ihre Integralwerte längs gewisser Mannigfaltigkeiten*, Berichte Sächsische Akademie der Wissenschaften zu Leipzig, Math.-Phys. Kl., **69** (1917), pp. 262–277. (translated : *On the Determination of Functions from Their Integral Values along Certain Manifolds*, in IEEE Trans. Med. Imaging, **MI-5** (1986), pp. 170–176.)

[12] P. A. Toft, *The Radon Transform — Theory and Implementation*, Ph.D. Thesis, Technical University of Denmark, 1996.